DOI: 10.1002/asia.201500597

CHEMISTRY
AN ASIAN JOURNAL
Communication

Charge Transfer

Indolizino[5,6-*b*]quinoxaline Derivatives: Intramolecular Charge Transfer Characters and NIR Fluorescence

Mitsuru Kojima,[a] Hironobu Hayashi,[a] Tatsuya Aotake,[a] Shinya Ikeda,[a] Mitsuharu Suzuki,[a] Naoki Aratani,[a] Daiki Kuzuhara,[a] and Hiroko Yamada*[a, b]

Abstract: Indolizino[5,6-*b*]quinoxaline derivatives (**1a** and **1b**) with a push–pull structure were prepared to show intramolecular charge-transfer properties. Compounds **1a** and **1b** are strongly fluorescent in aprotic solvents while symmetrical derivatives (**2a** and **2b**) were non-fluorescent. The π-expanded α–α linked dimer (**10**) of indolizino[5,6-*b*]quinoxaline **1b** was serendipitously obtained to show NIR absorption over 800 nm and the fluorescence edge reached to 1400 nm.

Quinoxalines are electron-deficient heteroaromatic rings and have less negative reduction potential than the corresponding aromatic hydrocarbons. Quinoxalines are one of the most common building blocks used for electron transport materials for organic light-emitting diodes with high fluorescence quantum yields[1–6] and for the new electron acceptors in organic solar cells by attaching with fullerene.[7] Due to their facile synthesis and derivatization, various quinoxaline-based fluorophores were designed, founded on π-expansion and introduction of substituents.[8–10] In order to use quinoxaline compounds for near-infrared (NIR) fluorophores, we envisioned the construction of intramolecular charge-transfer (ICT) character by fusing the electron-poor quinoxaline and electron-rich pyrrole to create an aromatic ring incorporating a push–pull structure. To the best of our knowledge, the framework of indolizino[5,6-*b*]quinoxaline (**1a**) has not been reported (Figure 1), while pyrrole[1,2-*a*]quinoxalines,[11] pyrrole[2,3-*b*]quinoxalines,[12] and pyrrole[3,4-*b*]quinoxalines[13] have been reported in the field of pharmaceutical agents. Density functional theory (DFT) calculation at the B3LYP/6-31G(d) level of theory using the Gaussian 09 software package[14] suggested that the contribution of the pyrrole moiety for the HOMO is stronger than that of the quinoxaline moiety, whereas the contribution of the quinoxaline moiety for the LUMO is stronger than that of the pyrrole moiety (Figure 2). In addition to quinoxaline-pyrrole fused compound **1a**, we also prepared dipyrrolo[1′,2′:1,6;1″,2″:4,5]pyrazino[2,3-*b*]quinoxaline (**2a**) to compare the electronic structures of the molecules. Compounds **1a** and **2a** were expected to be planar showing strong π–π interaction in the solid state, and thus we have introduced the bicyclo[2.2.2]octadiene (BCOD) framework at the 3,4-position of pyrroles to give 8,11-dihydro-8,11-ethanobenzo[1,2]-indolizi-

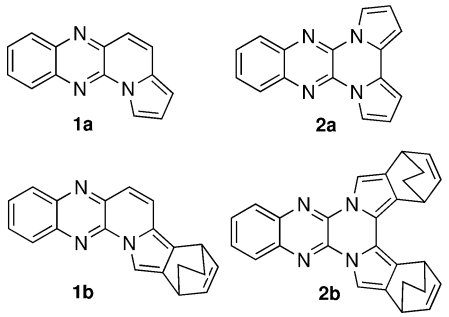

Figure 1. Structures of the indolizino[5,6-*b*]quinoxaline compounds. **1b** and **2b** are mixtures of stereoisomers.

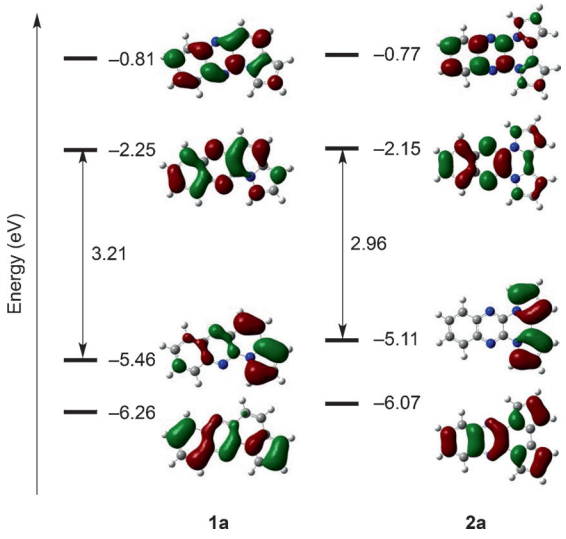

Figure 2. Molecular orbitals of **1a** and **2a** calculated at the B3LYP/6-31G(d) level of theory.

[a] *M. Kojima, Dr. H. Hayashi, Dr. T. Aotake, Dr. S. Ikeda, Dr. M. Suzuki, Prof. Dr. N. Aratani, Dr. D. Kuzuhara, Prof. Dr. H. Yamada*
Graduate School of Materials Science
Nara Institute of Science and Technology
8916-5 Takayama-cho, Ikoma, Nara 630-0192 (Japan)
E-mail: hyamada@ms.naist.jp

[b] *Prof. Dr. H. Yamada*
CREST
Japan Science and Technology Agency (JST)
4-1-8 Honcho, Kawaguchi, Saitama 332-0012 (Japan)

Supporting information for this article is available on the WWW under http://dx.doi.org/10.1002/asia.201500597.

no[5,6-*b*]quinoxaline (**1b**) and 8,11,12,15-tetrahydro-8,11:12,15-diethanodiisoindolo- [2′,1′:1,6;2″,1‴:4,5]pyrazino-[2,3-*b*] quinoxaline (**2b**) to prevent π–π stacking in the solid state. We report here the synthesis, single-crystal structures, and optical properties of indolizino[5,6-*b*]quinoxalines **1a** and **2a** as well as of their sterically hindered derivatives, **1b** and **2b**. We have also obtained the π-expanded α–α linked dimer (**10**) of indolizino[5,6-*b*]quinoxaline **1b** serendipitously by heating **1b** to proceed in a retro-Diels–Alder reaction. The dimer **10** showed NIR fluorescence that reached 1400 nm.

The synthetic procedures of compounds **1** and **2** are shown in Scheme 1. Compound **1a** was prepared from 2,3-dibromoquinoxaline (**3**) in 5 steps. The treatment of **3** with 25% aqueous NH_3 gave 2-amino-3-bromoquinoxaline (**4**) in 80% yield.[12] The construction of the pyrrole ring on **4** by the Paal–Knorr method gave 2-bromo-3-(1*H*-pyrrol-1-yl)quinoxaline (**6a**) in 23% yield, and Sonogashira coupling of **6a** with trimethylsilylacetylene gave **7a** in 76% yield. The desilylation of **7a** with $Bu_4N^+F^-$ gave **8a** in 69% yield, and indium-catalyzed cyclization reaction of **8a** afforded **1a** in 28% yield.[15] The preparation of compound **1b** was started from the coupling of **3** and bicyclo[2.2.2]octadienylpyrrole (**5**)[16] in 23% yield to give **6b**. Compound **1b** was prepared from **6b** in 3 steps by using the same method as for the synthesis of **1a**. Compounds **2a** and **2b** were prepared from **3** in 2 steps: treatment of **3** with pyrrole or **5** in the presence of NaH afforded **9a** and **9b** in yields of 82% and 74%, respectively. The subsequent oxidative intramolecular cyclization reaction between neighboring pyrrole rings by irradiation using a high-pressure mercury lamp (500 W) in the presence of I_2 afforded **2a** and **2b** in yields of 33% and 59%, respectively. Compounds **1b** and **2b** were obtained as a mixture of stereoisomers. The products were characterized by ^1H and ^{13}C NMR spectroscopy and ESI mass spectrometry.

Explicit structural determination of compounds **1a**, **1b**, **2a** and **2b** was carried out using X-ray crystallographic analysis as shown in Figure 3.[17] Compounds **1a** and **2a** show fairly planar frameworks with mean plane deviations of 0.01 Å and 0.03 Å from the plane defined by 17 and 20 atoms, respectively. In the packing structure, both compounds exhibit columnar structures with intermolecular distances of 3.349 and 3.309 Å, respectively, between the planes of two neighboring molecules, suggesting effective π–π interactions. In each column, head-to-head rearrangement was observed, which suggests that the electron-poor quinoxaline unit and the electron-rich pyrrole unit are each arranged in a line. For compounds **1b** and **2b**, the indolizino[5,6-*b*]quinoxaline skeletons are planar, but the columnar structures are disturbed. Compound **1b** shows a block structure with four alternately π–π stacked molecules, but the blocks are independent and do not form a columnar structure (Figure S1 a, Supporting Information). Compound **2b** shows a pair of alternately stacked molecules, and each pair does not show π–π interaction with another pair (Figure S1 b).

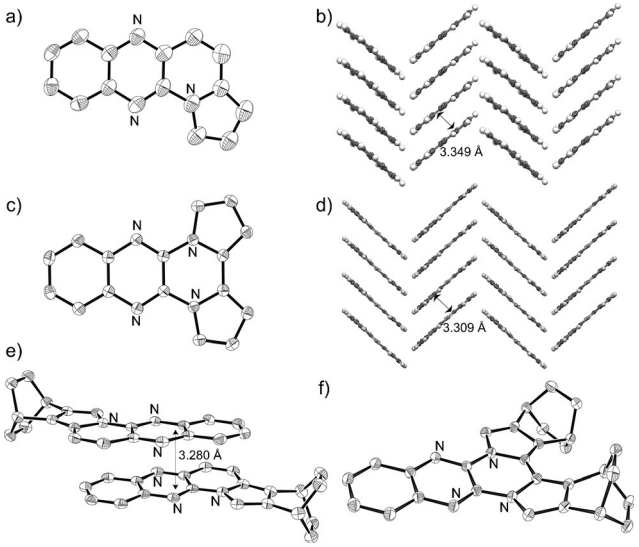

Figure 3. Single-crystal X-ray structures and packing structures of compounds **1a** (a and b), **2a** (c and d), **1b** (e), and **2b** (f). Thermal ellipsoids are shown at 50% probability. Hydrogen atoms were omitted for clarity.

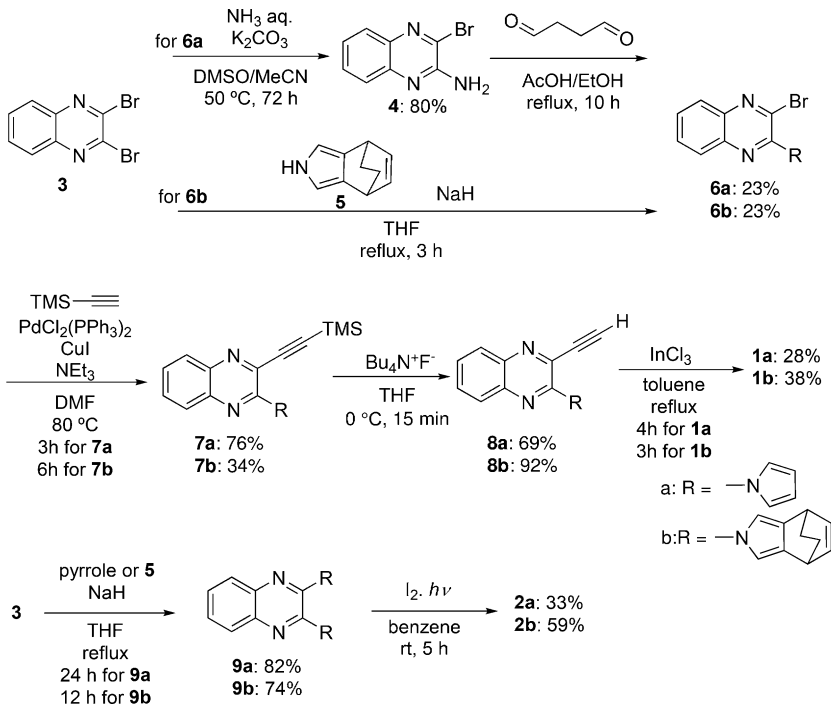

Scheme 1. Synthetic routes of **1a**, **1b**, **2a**, and **2b**.

are shown in Figure 4a. Compound **1a** in CH_2Cl_2 absorbs at 305, 365, 381, and 438 nm. Compared to benzo[*a*]anthracene (λ_{abs} = 386 nm),[18] the absorption maximum of **1a** is red-shifted by about 50–60 nm. This indicates that the push–pull indolizino[5,6-*b*]quinoxaline structure is suitable to narrow the HOMO–LUMO band gap. Compound **1b** absorbs around 313, 403, and 460 nm, and the red-shift of **1b** was enhanced compared to **1a** due to the electron-donating alkyl substituents on the electron-rich pyrrole moiety. Compound **2a** (and **2b**) exhibits strong absorption at 367 and 385 (383 and 402) nm, with a weak broad absorption reaching 550 nm. The strong absorption of **2b** at 386 nm is red-shifted by 17 nm compared to that of **2a** due to the alkyl substituents. From the time-dependent (TD) DFT calculations of compounds **1a** and **2a** at the B3LYP/6-31G(d) level, the intense absorption at 438 nm of **1a** and the broad absorption around 400–550 nm of **2a** are attributed to the transition from the HOMO to the LUMO with ICT character (Figures S2 and S3, Supporting Information). The overlap of the HOMO and the LUMO of **2a** and **2b** is not effective, and the molar extinction coefficient for π–π* transition is relatively weak (**2a**: 1832 $M^{-1}cm^{-1}$ at 419 nm, **2b**: 2460 $M^{-1}cm^{-1}$ at 440 nm).

Compounds **1a** and **1b** in CH_2Cl_2 showed strong fluorescence at 532 nm (Φ_F = 75%) and 542 nm (Φ_F = 70%) with fairly large Stokes shifts of 4086 and 3336 cm^{-1}, respectively (Figure 4a). To shed light on the contribution of ICT character in compounds **1a** and **1b**, the absorption and fluorescence spectra of compounds **1a** and **1b** were measured in various solvents (Figure 4b and S4) and analyzed by using Lippert–Mataga plots (Figure 4c).[19] The data are summarized in Table 1. The $\lambda_{abs}/\lambda_{em}$ values of **1a** varied from 441/522 nm (in toluene) to 435/537 nm (in acetonitrile), and the Stokes shifts ($\Delta\nu = \nu_{abs} - \nu_{em}$) of **1a** greatly increased with increasing orientation polarizability (Δf) of the solvent. As shown in Figure 4c, the Lippert–Mataga analyses gave linear solvation energy relationships (LSERs) versus the Δf values (R = 0.84 and 0.80 in each case). The LSERs of **1a** ($\Delta\nu/\Delta f = 2.8\times10^3$ cm^{-1}) and **1b** ($\Delta\nu/\Delta f = 3.5\times10^3$ cm^{-1}) are comparable. Compounds **2a** and **2b** showed no fluorescence in the solvents used for **1a** and **1b**.

Table 1. Photophysical data of compounds **1a** and **1b** in various solvents.

	Solvents	λ_{abs}[a] [nm]	λ_{em}[b] [nm]	Φ_F [%]	Stokes Shift [cm^{-1}]
1a	Toluene	441	522	75	3519
	$CHCl_3$	444	532	68	3726
	THF	439	526	73	3768
	CH_2Cl_2	437	532	75	4086
	DMF	440	539	63	4174
	CH_3CN	435	537	57	4367
	CH_3OH	441	569	9	5101
1b	Toluene	458	521	80	2640
	$CHCl_3$	462	543	67	3229
	THF	457	529	75	2978
	CH_2Cl_2	459	542	70	3336
	DMF	458	544	63	3452
	CH_3CN	453	548	55	3827
	CH_3OH	462	576	8	4284

[a] The longest absorption peaks; [b] $\lambda_{Ex} = \lambda_{abs}$.

The fluorescence quantum yields (Φ_F) of **1a** in aprotic nonpolar solvents such as toluene, THF, and CH_2Cl_2 are around 75%, while they are about 60% in aprotic polar solvents such as DMF and CH_3CN. In protic methanol, Φ_F decreased dramatically to 9%. A similar trend was observed for compound **1b**. To gain more insights into the fluorescence behavior of the compounds, the fluorescence lifetimes of **1a** and **1b** were also measured in toluene, CH_2Cl_2, and methanol (Figure S5 and Table S2, Supporting Information). The fluorescence decay was reasonably fitted to a single exponential model. The fluorescence lifetimes of **1a** and **1b** were 11.6 and 9.9 ns in toluene, 13.8 and 11.8 ns in CH_2Cl_2, and 2.5 and 1.4 ns in methanol, respectively. Thus, the lifetimes in toluene and CH_2Cl_2 are about 5 times longer than those in methanol. The fluorescence of **1a** as a solid was not detected, while fluorescence of **1b** was observed at 638 and 686 nm, and the Φ_F was 5.5% (Figure S6, Supporting Information). Although the BCOD moiety improves

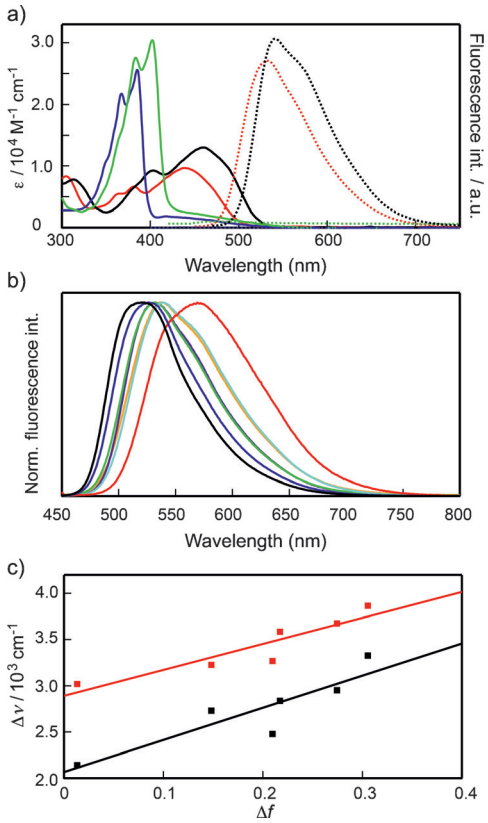

Figure 4. (a) Absorption (solid lines) and fluorescence (dotted lines) spectra of compound **1a** (red), **1b** (black), **2a** (blue), and **2b** (green) in CH_2Cl_2. (b) Normalized fluorescence spectra of compound **1a** in toluene (black), $CHCl_3$ (purple), THF (blue), CH_2Cl_2 (green), DMF (cyan), CH_3CN (orange), and methanol (red). All compounds were excited at their corresponding longest λ_{max}. (c) Lippert–Mataga plots for the solvatochromism of compounds **1a** (red) and **1b** (black) in toluene, $CHCl_3$, THF, CH_2Cl_2, DMF, and CH_3CN. $\Delta\nu = \nu_{abs} - \nu_{em}$, calculated from the data listed in Table 1. $\Delta f = (\varepsilon\text{-}1)/(2\varepsilon+1)\text{-}(n^2\text{-}1)/(2n^2+1)$. ε = dielectric constant; n = refractive index.

the fluorescence quantum yield in the solid, π–π stacking of **1b** is relatively strong as shown in Figure 3e and S1.

The thermogravimetric analysis of compound **1b** is shown in Figure S7 in the Supporting Information. The retro-Diels–Alder reaction of the BCOD moiety occurred at around 200 °C, but the product seemed unstable. Compound **1b** was heated to 200 °C as a solid to try a retro-Diels–Alder reaction, and subsequently a trace amount of a new compound with a molecular weight of 536.1733 was detected by MALDI-TOF mass spectrometry. To improve the reaction conditions, compound **1b** was heated for 30 min in DMSO by using a microwave to give compound **10** in 11% yield (Scheme 2). The compound was

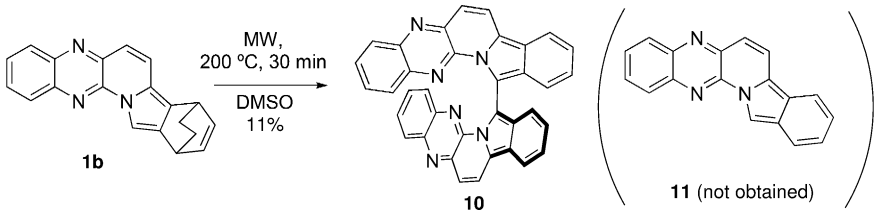

Scheme 2. Synthetic route of dimer **10**.

unstable when exposed to light, and purification was done under red light. Compound **10** was characterized by ^{1}H NMR spectroscopy, HR-MALDI-TOF mass spectrometry, and single-crystal X-ray structural analysis, as shown in Figures 5 and S8. The data confirmed that a retro-Diels–Alder reaction at the BCOD moiety and oxidative homo-coupling reaction at the α-position of pyrrole moiety occurred. The bond between C1 and C19 is a single bond with a length of 1.444(2) Å. The dihedral angle between the two indolizine units is 53.72°. The π–π distances between the intermolecular quinoxaline rings in the crystal are 3.296 and 3.292 Å, which suggests π–π interaction between the adjoining quinoxaline rings. The coupling reaction of compound **1a** was not successful, neither upon heating to 200 °C in the solid state nor upon irradiation in a microwave in DMSO.

The UV/Vis absorption and fluorescence spectra of compound **10** in CH_2Cl_2 are shown in Figure 5 with the oscillator

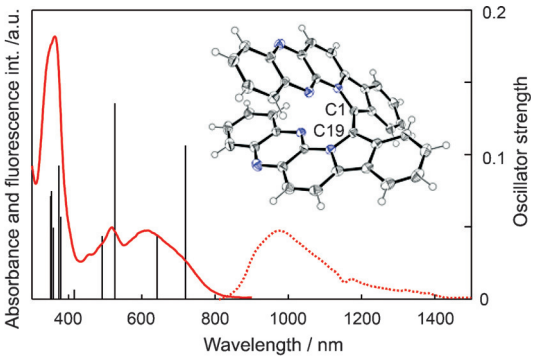

Figure 5. Normalized absorption (solid red line) and fluorescence intensity (dotted red line) in CH_2Cl_2. The calculated oscillator strength is also shown as black lines. Fluorescence was measured with λ_{Ex} = 600 nm.

strength calculated at B3LYP/6-31G(d) level of theory. The absorption peaks were observed at 362, 519, and 614 nm, and the edge reaches to 800 nm. Molecular orbitals and energy levels of compound **10** and the corresponding monomer **11** are shown in Figure S10 in the Supporting Information. The HOMO–LUMO energy difference of **10** is smaller than those of **1a**, **1b**, and **11** due to the expanded π-conjugation. The HOMO level of **10** is almost 1 eV higher than that of **1a** because of the π-expanded structure of the HOMO of **10**. Therefore, **10** is quite unstable under room light. The fluorescence peak of **10** was observed at 975 nm in CH_2Cl_2 and the edge reached to 1400 nm. The polarity of the solvents has little effect on the wavelength of absorption and emission peaks (Figure S9). The Stokes shift of compound **10** is 6030 cm^{-1}, a value much larger than those of **1a** and **1b** because of the rotation of **10** around the C1–C19 single bond.

In summary, indolizino[5,6-*b*]quinoxaline derivatives with a fusion of an electron-poor quinoxaline and electron-rich pyrrole have been prepared for the first time. Compounds **1a** and **1b** showed ICT character and Φ_F of 50–80% in aprotic solvents, while **2a** and **2b** did not show any fluorescence. The dimer **10** was obtained only by heating of **1b**, and the fluorescence edge of **10** was found to reach to 1400 nm because of the expansion of π-conjugation by the fused benzene ring and dimerization. Compounds **1** and **2** are relatively unstable because the α-position of the pyrrole moiety does not have a substituent, and compound **11** could not be isolated. However, considering the strong fluorescence and π–π interaction in the crystal structure of compound **1a**, the α-substituted indolizino[5,6-*b*]quinoxaline will be promising for optoelectronic materials. Further derivatization of indolizino[5,6-*b*]quinoxalines is currently undergoing in our laboratory.

Acknowledgements

This work was partly supported by Grants-in-Aid for Scientific Research (KAKENHI) Nos. 25288092, 26620167, 26105004 and 15H00876 ('AnApple') from the Japan Society for the Promotion of Science (JSPS), and the program for promoting the enhancement of research universities in NAIST supported by the Ministry of Education, Culture, Sports, Science and Technology (MEXT). We thank Ms. A. Kuramoto, Ms. Y. Nishikawa, Mr. Y. Okajima and Mr. S. Katao at NAIST for help in absorption and emission measurement, mass spectrometry, fluorescence lifetime measurement, and single-crystal X-ray diffraction analysis, respectively.

Keywords: intramolecular charge transfer · pyrrole · quinoxaline · single-crystal structure · solvent effects

[1] K. R. J. Thomas, J. T. Lin, Y.-T. Tao, C.-H. Chuen, *Chem. Mater.* **2002**, *14*, 3852 – 3859.
[2] A. P. Kulkarni, Y. Zhu, S. A. Jenekhe, *Macromolecules* **2005**, *38*, 1553 – 1563.
[3] C.-T. Chen, Y. Wei, J.-S. Lin, M. V. R. K. Moturu, W.-S. Chao, Y.-T. Tao, C.-H. Chien, *J. Am. Chem. Soc.* **2006**, *128*, 10992 – 10993.
[4] H. D. Burrows, S. M. Fonseca, B. Gigante, M. A. Esteves, A. M. Guerreiro, *J. Fluoresc.* **2006**, *16*, 227 – 231.
[5] Y. Wei, S. Samori, S. Tojo, M. Fujitsuka, J.-S. Lin, C.-T. Chen, T. Majima, *J. Am. Chem. Soc.* **2009**, *131*, 6698 – 6707.
[6] Q. Miao, *Adv. Mater.* **2014**, *26*, 5541 – 5549.
[7] a) W. Chen, Q. Zhang, T. Salim, S. A. Ekahana, X. Wan, T. C. Sum, Y. M. Lam, A. H. H. Cheng, Y. Chen, Q. Zhang, *Tetrahedron* **2014**, *70*, 6217 – 6221; b) W. Chen, T. Salim, H. Fan, L. James, Y. M. Lam, Q. Zhang, *RSC Adv.* **2014**, *4*, 25291 – 25301.
[8] K. Kudo, A. Momotake, Y. Kanna, Y. Nishimura, T. Arai, *Chem. Commun.* **2011**, *47*, 3867 – 3869.
[9] H.-J. Son, W.-S. Han, D.-H. Yoo, K.-T. Min, S.-N. Kwon, J. Ko, S. O. Kang, *J. Org. Chem.* **2009**, *74*, 3175 – 3178.
[10] C. F. Gers, J. Nordmann, C. Kumru, W. Frank, T. J. J. Müller, *J. Org. Chem.* **2014**, *79*, 3296 – 3310.
[11] a) X.-C. Zhang, W.-Y. Huang, *Tetrahedron* **1998**, *54*, 12465 – 12474; b) K. Kobayashi, T. Matoba, S. Irisawa, T. Matsumoto, O. Morikawa, H. Konishi, *Chem. Lett.* **1998**, 551 – 552; c) G. Campiani, A. Cappelli, V. Nacci, M. Anzini, S. Vemero, M. Hamon, A. Cagnotto, C. Fracasso, C. Uboldi, S. Caccia, S. Consolo, T. Mennini, *J. Med. Chem.* **1997**, *40*, 3670 – 3678.
[12] A. Arcadi, S. Cacchi, G. Fabrizi, L. M. Parisi, *Tetrahedron Lett.* **2004**, *45*, 2431 – 2434.
[13] R. Kreher, G. Use, *Tetrahedron Lett.* **1978**, *19*, 4671 – 4674.
[14] Gaussian 09, Revision D.01, M. J. Frisch, G. W. Trucks, H. B. Schlegel, G. E. Scuseria, M. A. Robb, J. R. Cheeseman, G. Scalmani, V. Barone, B. Mennucci, G. A. Petersson, H. Nakatsuji, M. Caricato, X. Li, H. P. Hratchian, A. F. Izmaylov, J. Bloino, G. Zheng, J. L. Sonnenberg, M. Hada, M. Ehara, K. Toyota, R. Fukuda, J. Hasegawa, M. Ishida, T. Nakajima, Y. Honda, O. Kitao, H. Nakai, T. Vreven, J. A. Montgomery, Jr., J. E. Peralta, F. Ogliaro, M. Bearpark, J. J. Heyd, E. Brothers, K. N. Kudin, V. N. Staroverov, R. Kobayashi, J. Normand, K. Raghavachari, A. Rendell, J. C. Burant, S. S. Iyengar, J. Tomasi, M. Cossi, N. Rega, J. M. Millam, M. Klene, J. E. Knox, J. B. Cross, V. Bakken, C. Adamo, J. Jaramillo, R. Gomperts, R. E. Stratmann, O. Yazyev, A. J. Austin, R. Cammi, C. Pomelli, J. W. Ochterski, R. L. Martin, K. Morokuma, V. G. Zakrzewski, G. A. Voth, P. Salvador, J. J. Dannenberg, S. Dapprich, A. D. Daniels, Ö. Farkas, J. B. Foresman, J. V. Ortiz, J. Cioslowski, and D. J. Fox, Gaussian, Inc., Wallingford CT, **2009**.
[15] V. Mamane, P. Hannen, A. Fürstner, *Chem. Eur. J.* **2004**, *10*, 4556 – 4575.
[16] S. Ito, T. Murashima, H. Uno, N. Ono, *Chem. Commun.* **1998**, 1661 – 1662.
[17] CCDC 929004, 927909, 927911, 927910 and 1038091 contain the supplementary crystallographic data for this paper. These data are provided free of charge by The Cambridge Crystallographic Data Centre. Cryatallographic data for **1a**: C_{14} H_9 N_3, $Mw = 219.25$; orthorhombic; space group $P2_12_12_1$ (No. 19); $a = 4.4245(6)$ Å, $b = 13.256(2)$ Å, $c = 17.600(3)$ Å; $V = 1032.3(3)$ Å^3; $Z = 4$; $T = 103$ K, $\rho_{calcd} = 1.411$ g cm^{-3}; $R = 0.0628$, $wR_2 = 0.1675$ (all data). GOF = 1.014, CCDC No.: 929004. Cryatallographic data for **1b**: C_{40} H_{30} N_6, $Mw = 594.72$; monoclinic; space group $P2_1/n$ (No.14); $a = 13.7495(4)$ Å, $b = 12.5320(3)$ Å, $c = 18.1615(5)$ Å, $\beta = 113.1872(7)^\circ$; $V = 2876.6(2)$ Å^3; $Z = 4$; $T = 103$ K, $\rho_{calcd} = 1.373$ g cm^{-3}; $R = 0.0590$, $wR_2 = 0.1326$ (all data). GOF = 1.086, CCDC No.: 927909; Cryatallographic data for **2a**: C_{16} H_{10} N_4, $Mw = 258.28$; monoclinic; space group $P2_1/n$ (No.14); $a = 4.55445(1)$ Å, $b = 17.3451(5)$ Å, $c = 15.1147(5)$ Å, $\beta = 94.9123(7)^\circ$; $V = 1189.64(6)$ Å^3; $Z = 4$; $T = 123$ K, $\rho_{calcd} = 1.442$ g cm^{-3}; $R = 0.0488$, $wR_2 = 0.1068$ (all data). GOF = 1.085, CCDC No.: 927911; Cryatallographic data for **2b**: C_{28} H_{22} N_4, $Mw = 414.51$; triclinic; space group P-1 (No.2); $a = 9.6713(3)$ Å, $b = 10.0384(3)$ Å, $c = 11.6538(4)$ Å, $\alpha = 65.1315(7)^\circ$, $\beta = 76.2275(8)^\circ$, $\gamma = 78.7426(8)^\circ$; $V = 991.16(5)$ Å^3; $Z = 2$; $T = 103$ K, $\rho_{calcd} = 1.389$ g cm^{-3}; $R = 0.0569$, $wR_2 = 0.1840$ (all data). GOF 1.150, CCDC No.: 927910; Crystallographic data for **10**: $C_{36}H_{20}N_6$, $Mw = 536.59$; monoclinic; space group $P2_1/n$ (No.14); $a = 12.9175(3)$ Å, $b = 12.1457(3)$ Å, $c = 16.5562(4)$ Å, $\beta = 102.4428(7)^\circ$; $V = 2536.52(10)$ Å^3; $Z = 4$; $T = 103$ K, $\rho_{calcd} = 1.405$ g cm^{-3}; $R = 0.0435$, $wR_2 = 0.1122$ (all data). GOF = 1.081, CCDC No.: 1038091.
[18] B. B. Bhowmik, T. K. Paul, *Spectrochim. Acta Part A* **1984**, *40*, 601 – 606.
[19] Z. R. Grabowski, K. Rotkiewicz, W. Rettig, *Chem. Rev.* **2003**, *103*, 3899 – 4031.

Manuscript received: June 10, 2015
Accepted Article published: June 25, 2015
Final Article published: July 21, 2015